Toxicology 489 (2023) 153489

Contents lists available at ScienceDirect

Toxicology

journal homepage: www.elsevier.com/locate/toxicol

Ripretinib induced skeletal muscle toxicity through mitochondrial impairment in C2C12 myotubes

Tugce Boran [a,b], Ozge Sultan Zengin [a,c], Zehra Seker [c,d], Aysenur Gunaydin Akyildiz [d], Ezgi Oztas [a], Gül Özhan [a,*]

[a] Istanbul University, Faculty of Pharmacy, Department of Pharmaceutical Toxicology, 34116 Istanbul, Turkey
[b] Istanbul University-Cerrahpaşa, Faculty of Pharmacy, Department of Pharmaceutical Toxicology, 34500 Istanbul, Turkey
[c] Institute of Graduate Studies in Health Sciences, Istanbul University, 34116 Istanbul, Turkey
[d] Bezmialem Vakif University, Faculty of Pharmacy, Department of Pharmaceutical Toxicology, 34093 Istanbul, Turkey

ARTICLE INFO

Handling Editor:Dr. Mathieu Vinken

Keywords:
Ripretinib
Kinase inhibitors
Myotoxicity
Mitochondrial damage
C2C12 myotubes

ABSTRACT

Ripretinib is a multikinase inhibitor drug approved in 2020 by the FDA and in 2021 by EMA for use in the treatment of advanced gastrointestinal stromal tumors (GIST) which have not adequately responded to previous treatments with kinase inhibitors. The most common side effects of the drug are myalgia and fatigue, which likely causes interruption of the treatment or reduction of the dose. Skeletal muscle cells highly depend on ATP to perform their functions and mitochondrial damage may play a role in skeletal muscle toxicity induced by kinase inhibitors. However, the molecular mechanism has not been clearly identified in the literature yet. In this study, it has been aimed to elucidate the role of mitochondria in the toxic effect of ripretinib on skeletal muscle using the mouse C2C12 myoblast-derived myotubes. The myotubes were exposed to ripretinib at the range of 1–20 μM concentrations for 24 h. To determine the potential role of mitochondrial impairment in ripretinib-induced skeletal muscle toxicity, intracellular ATP level, mitochondrial membrane potential (MMP), mitochondrial ROS production (mtROS), mitochondrial DNA (mtDNA) copy number, and mitochondrial mass were examined after ripretinib treatment. Furthermore, changes in PGC 1α/NRF 1/NRF 2 expression levels that play a role in mitochondrial biogenesis and mitophagy were investigated. Additionally, the mitochondrial electron transport chain (ETC) enzyme activities were evaluated. Lastly, a molecular docking study was done to see ripretinib's possible interaction with DNA polymerase gamma (POLG) which is important for DNA replication in the mitochondria. According to the findings, ripretinib decreases the ATP level and mtDNA copy number, induces loss of MMP, and reduces mitochondrial mass. The activities of the ETC complexes were inhibited with ripretinib exposure which is in line with the observed ATP depletion and MMP loss. The molecular docking study revealed that ripretinib has inhibitory potential against POLG which supports the observed inhibition of mtDNA. The expression of PGC 1α was reduced in the nuclear fraction indicating that PGC-1α was not activated since the NRF 1 expression was reduced and NRF 2 level did not show significant change. Consequently, mtROS production increased in all treatment groups and mitophagy-related gene expressions and Parkin protein expression level were up-regulated at high doses. In conclusion, mitochondrial damage/loss can be one of the underlying causes of ripretinib-induced skeletal muscle toxicity. However, further studies are needed to confirm the results in vivo.

1. Introduction

Compared to conventional chemotherapy, kinase inhibitors target molecules specific to tumor growth and progression. Although the use of targeted therapies in cancer treatment is very promising, it has been reported that many organs and systems have been negatively affected with the increase in the use of kinase inhibitors (Hartmann et al. 2009). One of the common side effects of kinase inhibitors is their toxic effects on skeletal muscle which may cause an interruption of a successful cancer treatment. Ripretinib is a switch-control kinase inhibitor drug that inhibits some tyrosine kinases and serine/threonine kinases which play role in cancer development (FDA and CDER, 2020). Unlike other kinase inhibitor drugs, it binds to a region called the "switch pocket" of the kinase enzyme. This region differs between kinase enzymes;

* Correspondence to: Istanbul University, Faculty of Pharmacy, Beyazit Fatih, İstanbul 34116, Turkey.
E-mail address: gulozhan@istanbul.edu.tr (G. Özhan).

https://doi.org/10.1016/j.tox.2023.153489
Received 5 August 2022; Received in revised form 3 March 2023; Accepted 14 March 2023
Available online 16 March 2023

therefore, it is reported that they can provide more selective inhibition compared to other kinase inhibitors (GIST Support International, 2020).

Ripretinib was approved by the FDA in 2020 for use in the treatment of advanced GIST in patients who had previously received 3 or more kinase inhibitor treatments (FDA and CDER, 2020). It has been found to be effective against many of the KIT proto-oncogene receptor tyrosine kinase and platelet derived growth factor receptor A (PDGFRA) mutations that are frequently seen in GIST patients. Muscle disorders caused by kinase inhibitors have been evaluated as fatigue and weakness, and the adverse effects negatively affect the patient's quality of life and cause deterioration in treatment compliance (Bouitbir et al. 2020). Also, some kinase inhibitors cause muscle wasting (Rinninella et al. 2021). Common adverse effects (≥20 %) of ripretinib include myalgia and fatigue. It has been reported to cause myalgia in 32 %, muscle spasm in 15 %, and an increase in blood creatine phosphokinase in 21 % of the patients (Kumar et al. 2021). Myalgia has been reported as a cause of treatment interruption or dose reduction in patients, and severe myalgia has been reported in up to 1.2 % of patients (FDA and CDER, 2020). The molecular mechanism is not clearly known; however, *in vitro* studies have shown that skeletal muscle toxicity caused by imatinib, dasatinib, sorafenib, and sunitinib may be associated with impaired mitochondrial function (Bouitbir et al. 2020; Damaraju et al. 2018). Impairment of mitochondrial function in muscle cells, which need high amounts of ATP to perform their functions, is associated with many diseases (Martínez et al. 2017). The severity and frequency of toxic effects may increase with the increase in the patients receiving ripretinib treatment. For this reason, it is of great importance to determine the toxic effect mechanisms. Therefore, in our study, it was aimed to examine the toxic effects of ripretinib on a mouse C2C12 myoblast-derived myotubes cell model by focusing on mitochondrial pathways including intracellular ATP level, mitochondrial mass, mitochondrial superoxide level, mitochondrial complex activities, expression levels of Peroxisome proliferator-activated receptor gamma coactivator 1-alpha (PGC 1α), nuclear respiratory factor 1 (NRF 1) and nuclear respiratory factor 2 (NRF 2) transcription factors, which have a very important role in mitochondrial dynamics and mitochondrial protein synthesis. Voltage-dependent anion channel 1 (VDAC1) expression was also evaluated as a marker of mitochondrial mass. In addition, autophagy, which is indeed very important for muscle cells homeostasis, was investigated using an autophagy marker, along with the expression levels of genes involved in mitophagy. Lastly, a molecular docking study was done to see ripretinib's possible interaction with POLG which is important for DNA replication in the mitochondria.

2. Materials and methods

2.1. Cell culture procedure

2.1.1. Cell culture

C2C12 mouse myoblast cells (CRL-1772, ATCC, VA, USA) were grown in cell culture flasks in Dulbecco's Modified Eagle's Medium (DMEM) medium containing 10 % fetal bovine serum (FBS), 1 % penicillin-streptomycin-amphotericin. Cell culture medium was renewed every 2–3 days. Cells were sub-cultured when they reached % 50 confluence. C2C12 cells is a widely used experimental model to evaluate the effects of chemicals on skeletal muscle and show similarities with human skeletal muscle. The cells are able to differentiate into myotubes that have sarcomere and contractility (Wong et al. 2020; Kaminski et al. 2012).

2.1.2. Cell differentiation

Cells were grown in DMEM medium supplemented with 2 % horse serum and 1 % penicillin-streptomycin-amphotericin for 6 days after the cells become confluent. Cell culture medium was changed every 2–3 days during differentiation. C2C12 myoblast cells were planted in the appropriate number of microplates/flasks and waited until they were 80 %– 90 % confluent. Then, cells were grown for 6 days on DMEM media containing 2 % horse serum and 1% penicillin-streptomycin-amphotericin to differentiate. During this period, cells were morphologically observed (Fig. S1A) that morphologic structure of myoblasts changed to multinucleated myotubule. cell differentiation was also confirmed myogenin expression at protein level (Fig. S1B). Myogenin expression has been shown to increase, at early stage of differentiation, and then decreases late stage of differentiation (Okamoto et al. 2019).

2.1.3. Ripretinib treatment

Ripretinib (Selleckchem, Houston, USA) was dissolved in DMSO and myotubes were exposed to ripretinib at the range of 1–20 μM concentrations for 24 h. The C_{max} value of ripretinib was reported as 1.5 μM after single administration of 150 mg ripretinib, however, the C_{max} can be increased by 36 % when riptetinib is used with CYP enzyme inhibitors (FDA and CDER, 2020). Therefore, the studied concentrations were determined in the range of 1–20 μM which includes the possibilities. Ripretinib was dissolved in DMSO and cells were exposed to 0.05% DMSO in the control group.

2.2. Cytotoxicity

2.2.1. MTT assay

Following exposure to ripretinib, MTT solution (20 μL of 5 mg/mL MTT dye solution) was added to each well and incubated for 3 h at 37 °C in dark. At the end of incubation, supernatant was removed and DMSO was added to the wells to dissolve the formazan crystals. Optic density (OD) was measured using a microplate reader (Epoch, Germany) at 590 nm. Cell viability was calculated as a percentage of the control group.

2.2.2. LDH assay

LDH activity was determined with a commercial kit (Roche, Germany) according to the manufacturer's protocol. After ripretinib treatment, 96 well plate was centrifuged at 250 g for 2 min, then the cell culture supernatant (100 μL) was collected in a new 96-well plate and the reaction mixture (100 μL) was added to each well. The plate was incubated in the dark for 15 min at room temperature. Cells were exposed to triton X-100 (5 %) as the positive control. The absorbance value was determined with a microplate reader at 490 nm. Cell viability (%) was calculated according to the formula below.

$$100\text{-}\ [(OD_{sample} - OD_{low\ control}) / (OD_{high\ control} - OD_{low\ control})^{*}\ 100].$$

2.3. Intracellular ATP content

Intracellular ATP content was determined with a commercial kit (Abcam, UK) following the manufacturer's guideline. Detergent solution (50 μL) was added to each well in a 96 well plate and the plate was sealed and shaken in an orbital shaker for 5 min at 600 rpm. Substrate solution (50 μL) was added to each of the wells and the plate was shaken again. The plate was kept in the dark for 10 min. Luminescence was measured using a microplate reader (BioTek Synergy H1, Germany). The ATP content was calculated using a generated ATP standard curve. The protein content was measured with the Pierce BCA protein assay kit (Thermo Scientific, USA). The ATP content was divided to the protein content (ATP/protein ratio) and the results were normalized to the control group.

2.4. Mitochondrial membrane potential (MMP)

Changes in MMP were measured using the JC-1 dye (Invitrogen, Massachusetts, USA). JC-1 is a green-fluorescent cationic dye which deposits and forms red fluorescent JC-1 aggregates in healthy mitochondria. When MMP dissipates, JC-1 cannot form aggregates and therefore shows green fluorescent (Sivandzade et al. 2019). Decrease in red/green fluorescence ratio indicates MMP loss. After ripretinib treatment, cells were collected with trypsin and washed with PBS (1X). Then,

the JC-1 dye was added (2 μM-final concentration) and the cells were incubated for 15 min at 37 °C. After incubation, the cells were washed with PBS (1X) and were re-suspended in PBS (1X, 500 μL). The cells were exposed to 100 μM carbonyl cyanide 4-(trifluoromethoxy)phenylhydrazone (FCCP) for 30 min which was used as the positive control. Fluorescence intensity was measured using ACEA flow cytometry (San Diego, CA, USA) in FL-1 and FL-2 channels. Results were analyzed with Novoexpress software (ACEA, CA, USA). The loss of MMP was shown in proportion to the control group.

2.5. Mitochondrial oxidative damage

The amount of mtROS was investigated by the MitoSox red mitochondrial superoxide indicator dye (Invitrogen, Massachusetts, USA). After ripretinib treatment, MitoSOX red (2.5 μM solution prepared in PBS) was added and the cells were incubated at 37 °C for 10 min. Afterwards, the cells were washed with PBS (1X) and were re-suspended in PBS (1X) for fluorescence measurement. For positive control, cells were exposed to 500 μM H_2O_2 for 30 min. The fluorescence intensity of each sample was measured in the FL-1 channel using ACEA flow cytometry (San Diego, CA, USA). Results were analyzed with Novoexpress software (ACEA, CA, USA). Results were given as the percentage of median fluorescence intensity (MFI, %), which is calculated by dividing the MFI of the tested sample to the control group and multiplied by 100.

2.6. Mitochondrial mass

Mitochondrial mass was determined using the Mitotracker green dye (Invitrogen, Massachusetts, USA) which accumulates independent of MMP. After exposure to ripretinib, cells were collected with trypsinization. Following the washing steps, cells were re-suspended in PBS (1X) and the Mitotracker green dye was added to each sample (100 nm final concentration) and the cells were incubated for 15 min in the dark at 37 °C. At the end of incubation, cells were washed with PBS (1X) and were re-suspended in PBS (1X, 500 μL). Fluorescence intensity of each sample was measured in the FL-1 channel using ACEA flow cytometry (San Diego, CA, USA). Results were analyzed with Novoexpress software (ACEA, CA, USA) and results were given as a percentage of the control group's MFI value.

2.7. mtDNA copy number

To determine the number of mtDNA copy number, DNA isolation was performed with a commercial kit (Intron Biotechnology, South Korea) following the manufacturer's guideline. mtDNA copy number was determined in LightCycler 480 (Mannheim, Germany) using OneScript Plus Reverse Transcriptase syber green (abmGood, Vancouver, Canada) with 100 ng DNA in the final 20 μL reaction mix using mtDNA and nuclear DNA primers (Table S). Results were calculated as previously stated by Quiros et al. 2017, and shown after normalization to the control group.

2.8. Measurement of the activity of mitochondrial complex I, II, IV, and V

Mitochondrial complex I, II, IV, and V activities were measured in bovine heart mitochondria using MitoTox™ Complex I, Complex II, Complex IV, and Complex V Activity Assay Kits (Abcam, UK) according to the manufacturer's instructions. Rotenone, 2-thenoyltrifluoracetone (TTFA), potassium cyanide (KCN) and oligomycin were used as the positive controls, respectively. In the control group, the bovine heart mitochondria were exposed to the same amount of DMSO found in the test wells. The enzyme activities of the treatment groups were calculated as a percentage of the control group, where the control group is 100 %.

2.9. Gene and protein expression levels

After ripretinib treatment, the cells were collected with trypsin. Total RNA isolation was carried out using the High Pure RNA Isolation Kit (Roche, Switzerland) according to the protocol given by the manufacturer. After determining the amount and purity of isolated RNAs using Take3 plate (Epoch, Germany), cDNA synthesis was performed with OneScript Plus cDNA Synthesis Kit (abmGood, Vancouver, Canada). Gene expression levels were quantified in LightCycler 480 (Mannheim, Germany) using OneScript Plus Reverse Transcriptase syber green (abmGood, Vancouver, Canada) with 100 ng cDNA in the final 20 μL reaction mix. The housekeeping gene was *β-actin*. Results were calculated as described by Livak and Schmittgen, (2001) and were normalized to the control group. Primer sequences are shown in Supplementary material (Table S).

Total protein isolation was performed using RIPA Lysis Buffer System (Santa Cruz Biotechnology, Texas, USA) following the instructions provided by the manufacturer. Protein quantification was performed using Pierce BCA Protein Assay Kit (Thermo Scientific, Massachusetts, USA). Nuclear fractions were isolated using a commercial kit (Bio Basic, Markham, Canada) following the manufacturer's rules. The protein level was measured using the Bradford reagent (Biorad, CA, USA). The expression levels of the identified proteins were investigated using the western blot method. Protein (20 μg) was mixed with sample buffer (Invitrogen, Massachusetts, USA) and sample reducing agent (Invitrogen, Massachusetts, USA), and were separated according to their molecular weight by electrophoresis in SDS gel (12 %). Proteins were transferred to PVDF membrane (Biorad, CA, USA) using a wet blotting system. Then, the membrane was blocked with non-fat dry milk (5 %) in TBST and incubated overnight at + 4 °C with a primary antibody. After incubation, the membrane was washed three times and was incubated at room temperature with horseradish peroxidase (HRP) conjugated anti-mouse secondary antibody (Abcam, UK). Protein bands were imaged on a chemiluminescence imaging device using the SuperSignal West Dura Extended Duration Substrate (Thermo Scientific, Massachusetts, USA). Results were densitometrically analyzed using Image J software (National Institute of Health, USA). β-actin was used as the cellular reference protein and histone 3 was used as reference protein for nuclear fractions. The primary antibodies used in the study were as follows; PGC 1α (Proteintech, IL, USA), NRF 1 (Santa Cruz Biotechnology, Texas, USA), NRF 2 (Proteintech, IL, USA), VDAC1 (Santa Cruz Biotechnology, Texas, USA), SOD2 (Santa Cruz Biotechnology, Texas, USA), TRX2 (Santa Cruz Biotechnology, Texas, USA), Parkin (Thermo Scientific, Massachusetts, USA), β-actin (Santa Cruz Biotechnology, Texas, USA) and Histone 3 (Active motif, CA, USA).

2.10. Molecular docking study

POLG is responsible for mitochondrial DNA replication, which is particularly susceptible to inhibition by zalcitabine, used as a structural basis for POLG-mediated drug toxicity (Szymanski et al. 2015). The crystal structure of POLG complexed with its inhibitor zalcitabine at 3.44 Å resolution (PDB ID: 4ZTZ) was retrieved from the RCSB Protein Data Bank. The docking study was carried out using the Schrödinger Software Suite (Maestro Schrödinger Release 2022, NY, 2022). The crystal structures of the enzymes were prepared using the Protein Preparation Wizard Module of Schrödinger Software Suite (Maestro Schrödinger Release 2022, NY, 2022) (Madhavi Sastry et al. 2013). The retrieved crystal structure was optimized by removing water molecules, heteroatoms, and co-factors. The hydrogens, missing atoms, bonds, and charges were computed and corrected through Maestro. The studied molecules and the co-crystallized ligand zalcitabine were also prepared and optimized (generating various tautomers and ring conformations, assigning bond orders, and stereochemistries) using the LigPrep module. All the conformations generated were minimized using the OPLS4 forcefield. The receptor grid was generated around the co-crystalized

ligand of the enzyme to specify the binding site, where the grid box size was determined with the receptor Grid Generation implemented in Glide. The Glide docking was performed in the Standard Precision (SP) mode for 4ZTZ (Friesner et al. 2006, Friesner et al. 2004; Halgren et al. 2004).

2.11. Transmission electron microscope (TEM) imaging

Following 20 μM ripretinib treatment, the cells were collected with trysinization, washed with PBS (1X), and the cells were fixed using glutaraldehyde solution (2.5 %) at + 4 °C for 24 h. After glutaraldehyde fixation, the cells were wash with PBS (1X) five times, then fixed in OsO_4 (1 %) for 1 h. Following washing steps, the cells were embedded in agar (4 %) and agar block were dehydrated with different concentration ethanol and agar block were embedded in resin. Ultra-thin sections were taken using an ultramicrotome (Leica, Germany). The sections were examined using FE-SEM microscope in STEM mode (Hitachi Regulus 8230, Japan).

2.12. Statistical analysis

Statistical analysis was performed using Graphpad Prism 6 (GraphPad Software Inc, CA, USA). Statistical differences were evaluated with one-way ANOVA followed by the Tukey test. Results were represented as mean ± standard deviation (SD). *$p < 0.05$, **$p < 0.01$, ***$p < 0.001$, ****$p < 0.0001$ values were considered as statistically significant.

3. Results

3.1. Cytotoxic effect of Ripretinib on C2C12 myotubes

The IC_{50} value of ripretinib could not be calculated since ripretinib did not show a cytotoxic effect on the C2C12 myotubes, however, the cell viability decrement in the 20 μM concentration group was statistically significant in the MTT assay (Fig. 1).

3.2. Changes in intracellular ATP content, mitochondrial membrane potential (MMP), and mitochondrial ROS production after ripretinib treatment

Following 24 h exposure, intracellular ATP content decreased in a concentration-dependent manner. This decrease was found significant at 10 μM and 20 μM concentrations ($p < 0.01$). Likewise, MMP showed a concentration-dependent decrease after 24 h exposure and was found statistically significant at the highest concentration compared to the control group ($p < 0.05$). Furthermore, mtROS was observed to be increased significantly after all tested concentrations ($p < 0.0001$) (Fig. 2).

3.3. Alterations of mitochondrial mass and mtDNA copy number after ripretinib treatment

Mitochondrial mass of the cells decreased at the highest concentration ($p < 0.05$) while mtDNA copy number dose-dependently decreased; in particular, at 10 μM and 20 μM concentrations ($p < 0.05$) (Fig. 3).

3.4. Inhibitory potential of ripretinib on mitochondrial complex activities

While ripretinib did not cause significant difference in mitochondrial complex I activity ($p > 0.05$), the activity of complex II reduced significantly ($p < 0.001$) in a dose-dependent manner. Complex IV activity was decreased at high ripretinib concentrations where significant inhibition was observed at 20 μM concentration ($p < 0.05$). Complex V activity decreased in a dose-dependent manner, and it was significantly inhibited at 5 μM, 10 μM, and 20 μM concentrations compared with the control group ($p < 0.001$) (Fig. 4).

3.5. Effect of ripretinib on gene expression levels

3.5.1. Mitochondrial biogenesis and mass

PGC 1α gene expression significantly increased at ≥ 10 μM ($p < 0.05$). *NRF 2* gene expression did not show statistically significant change, whereas *NRF 1* was downregulated at ≥ 5 μM. *VDAC1* gene expression was also significantly downregulated at 20 μM (Fig. 5).

3.5.2. Mitophagy

The expressions of *p62* at 20 μM concentration and *BNIP3* at 10 μM and 20 μM were upregulated after ripretinib treatment. However, the expression levels of *BNIP3L* and *FUNDC1* were significantly increased only at 10 μM concentration (Fig. 6).

3.6. Effect of ripretinib on protein expression levels

PGC 1α expression at the protein level was dose-dependently induced ($p > 0.05$) in the total cell lysate. On the contrary, nuclear PGC 1α expression was observed to decrease in a dose-dependent manner and the decrease was statistically significant at 20 μM ($p < 0.01$) (Fig. 7).

NRF1 expression level decreased in a dose-dependent manner and was inhibited significantly after treatment with 5 μM, 10 μM, and 20 μM concentrations compared to the control group. NRF2 level did not show significant changes compared to the control group, however, there was a decrease in the 20 μM treatment group. Besides, VDAC1 expression decreased significantly only at 20 μM ($p < 0.01$). SOD2, TRX2 and Parkin protein levels were significantly induced at the highest concentration after ripretinib treatment ($p < 0.05$). The LC3B- II/LC3B I protein ratio, which is a marker of autophagy, increased significantly at 10 μM and 20 μM concentrations. On the other hand, the LC3B II/VDAC1

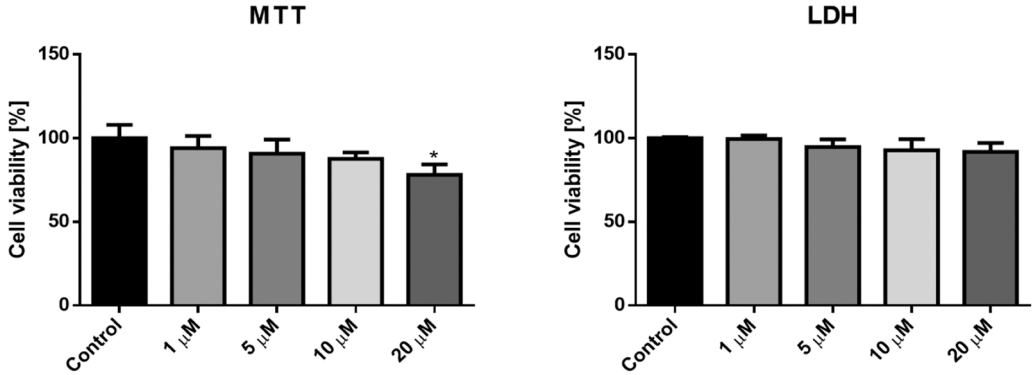

Fig. 1. Effect of ripretinib on cell viability of C2C12 myotubes after 24 h exposure. *$p < 0.05$ versus control group by MTT (3-(4,5-dimethylthiazol-2-yl)− 2,5-diphenyltetrazolium bromide) and LDH (lactate dehydrogenase) assays.

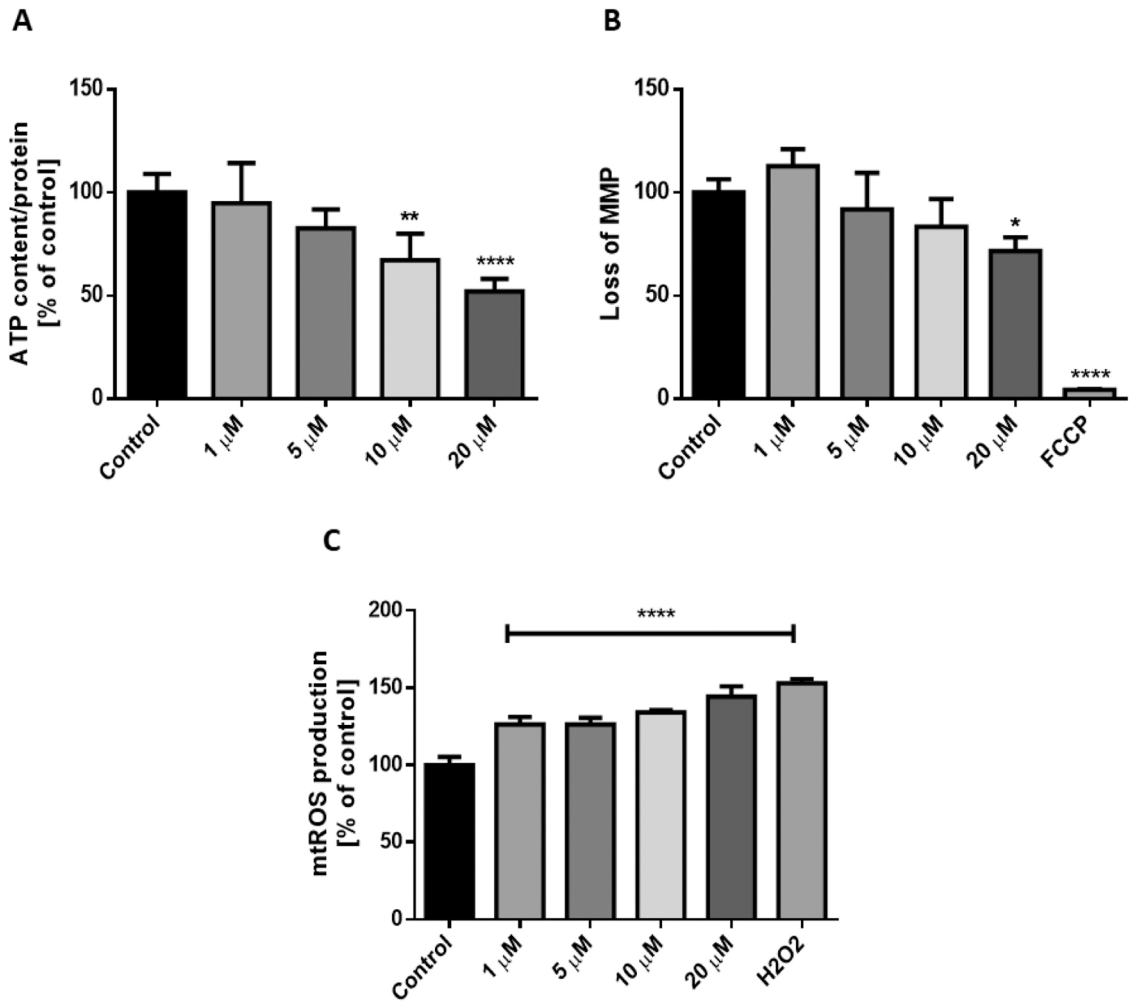

Fig. 2. Changes in ATP content (A), mitocohondrial membrane potential (MMP) (B), and mitochondrial ROS (mtROS) production (C) of C2C12 myotubes after 24 h ripretinib treatment. $*p < 0.05$, $**p < 0.01$, $****p < 0.0001$ versus control group. FCCP: carbonyl cyanide 4-(trifluoromethoxy) phenylhydrazone), H_2O_2: hydrogen peroxide (500 μM).

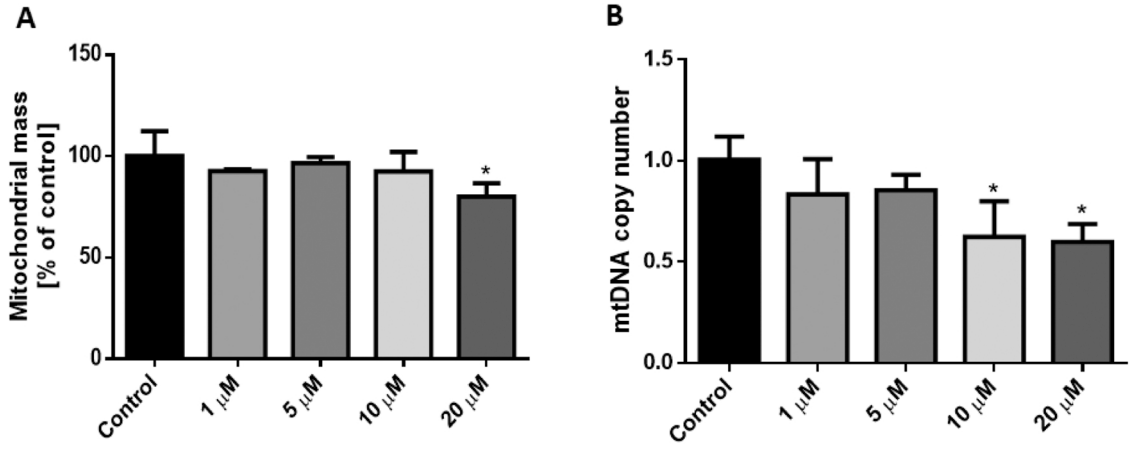

Fig. 3. Changes in mitochondrial mass (A) and mitochondrial DNA (mtDNA) copy number (B) after 24 h ripretinib treatment on C2C12 myotubes. $*p < 0.05$ versus control group.

protein ratio, which may be considered as a marker of mitophagy (Rao et al., 2022), was also increased at ≥ 10 μM concentrations (Fig. 8).

3.7. Molecular-docking study results

Molecular docking of ripretinib and other tyrosine kinase inhibitor drugs that are used in the treatment of GIST was carried out to POLG. The tyrosine kinase inhibitor drugs and their interactions with the

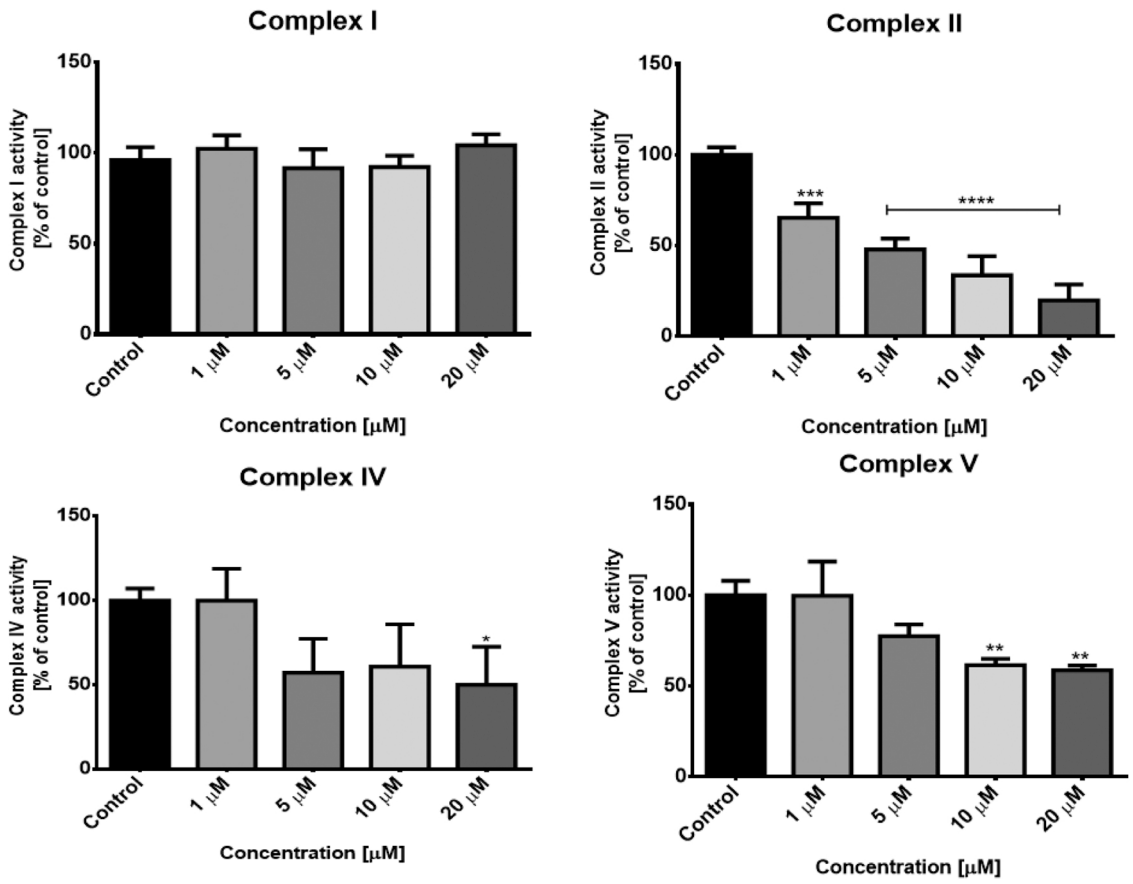

Fig. 4. Effects of ripretinib on mitochondrial complex I, II, IV, and V activities in bovine heart mitochondria. *$p < 0.05$, **$p < 0.01$, ***$p < 0.001$, ****$p < 0.0001$ versus control group.

binding site of 4ZTZ are given in Fig. 9 and Table 1. The docking score of ripretinib was determined as − 7.163 kcal/mol. In the active site of the receptor, ripretinib was found to interact with ARG853, LYS947, TYR951 amino acid residues, along with MG4001. The validation was done for the docking model and the Root mean square (RMS) value was found 0.733 by superpositioning the docked pose and experimental binding conformation of zalcitabine-TP in the binding pocket of 4ZTZ.

3.8. TEM imaging results

Mitochondrial damages including damaged cristae structure and membrane rupture were observed following 20 μM ripretinib exposure (Fig. 10A-B). Mitophagic and autophagic structures were also detected (Fig. 10B-D).

4. Discussion

The use of kinase inhibitor drugs as new generation anticancer agents as well as for other therapeutic purposes is increasing day by day. Many kinase inhibitor drugs have been reported to have toxic effects on the skeletal muscle. Although the toxic effect on the skeletal muscle may seem insignificant at the beginning, this may lead to a reduction in the treatment dose or to termination of the treatment even if the patient may have been benefiting from the treatment. In this study, it was aimed to investigate the toxic effects of ripretinib on the skeletal muscle using the C2C12 mouse myoblast-derived myotubule cell model which is a very suitable in vitro model for investigating skeletal muscle toxicity (Bouitbir et al. 2020; Damaraju et al. 2018).

The cytotoxicity of ripretinib was evaluated by two assays indicating the drug's toxicity according to mitochondrial toxicity and cellular membrane damage with the MTT and LDH assays, respectively. According to the results, ripretinib was observed to inhibit cell viability at 20 μM concentration in the MTT assay, which may suggest mitochondrial toxicity. Cell viability did not show significant changes in the LDH assay results.

Muscle cells need a quite lot of ATP in order to perform their contraction and relaxation functions, so any damage to mitochondria, which is the ATP production center, may negatively affect cellular functions (Kunz, 2001; Martínez et al. 2017). Indeed, mitochondrial dysfunction has been found to play a role in many skeletal muscle diseases (Gouspillou and Hepple, 2016). The results showed that ripretinib caused significant intracellular ATP depletion at 10 μM and 20 μM concentrations. two coordinated processes are involved in mitochondria for the ATP synthesis by oxidative phosphorylation. In these processes, mitochondrial complexes play crucial roles. Firstly, the transport of electrons across complexes in the inner mitochondrial membrane creates a proton gradient across the inner mitochondrial membrane. While electrons are transported across the complexes, protons in the mitochondrial matrix from complexes I, III and IV are pumped into the intermembrane space and a proton gradient is created across the inner membrane. For ATP synthesis, protons in the intermembrane space return to the matrix through ATP synthase (Complex V) and ATP synthesis takes place simultaneously. In this process, since the matrix is negative and the intermembrane space is positive, the difference in voltage and proton concentration creates a pH gradient between the two parts. These two conditions provide the formation of the MMP (Murphy et al. 2016). For these reasons, complexes' activities play a major role in the formation of MMP and ATP synthesis. The MMP is of great importance in the healthy production of ATP by the mitochondria (Zorova et al. 2018). In the present study, intracellular ATP content was reduced in a

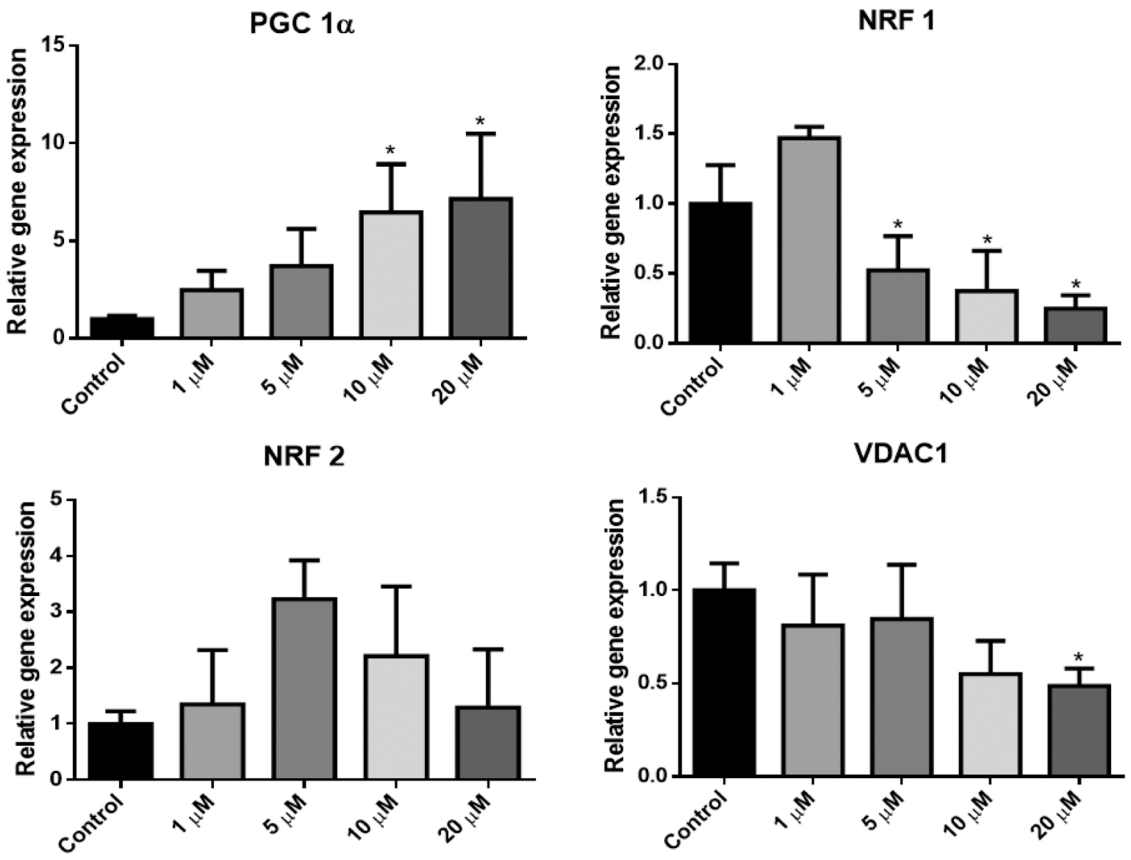

Fig. 5. Relative expressions of PGC 1α, NRF 1, NRF 2 and VDAC1 following 24 h ripretinib treatment. *$p < 0.05$ versus control group. PGC 1α: Peroxisome proliferator-activated receptor gamma coactivator 1-alpha, NRF 1/2: Nuclear respiratory factor 1/2, VDAC1: Voltage dependent anion channel 1.

dose-dependent manner and significant loss of MMP was observed. Also, ripretinib significantly diminished the activities of complex II, IV, and V. Namely, while the ripretinib-induced depletion of ATP may be through the inhibition of MMP and/or mitochondrial electron transport chain activities, vice versa, ripretinib may cause MMP inhibition leading to the inhibition of ATP synthesis along with inhibiting complex II, IV, and V (ATP synthase) in the myotubes.

It has been demonstrated that some kinase inhibitors cause mitochondrial dysfunction via loss of MMP, alterations of mitochondrial complex activities, and increase in mitochondrial ROS production (Bouitbir et al. 2020; Damaraju et al. 2018). Mitochondria are one of the main ROS producer in the cells (Murphy, 2009). Inhibiton of mitochondrial complexes may contribute to the mtROS production in the cell (Kokoszka et al. 2001; Okada et al. 2021, Atashbar et al. 2022). mtROS production was also observed to be increased after ripretinib treatment. Excessive mtROS production causes mitochondrial damage which may be associated with muscle atrophy (Min et al. 2011; Romanello and Sandri, 2016). SOD2 and TRX2 enzymes defend cells against oxidative stress in the mitochondria (Napolitano et al. 2021). In our study, SOD2 and TRX2 protein expression levels were significantly induced after 24 h ripretinib treatment at 20 μM concentration, which might be a protective response to mitochondrial damage and enhanced mtROS production. Similar to our findings, Bouitbir et al. 2020 reported the expressions of SOD2 and TRX2 proteins enhanced with dasatinib and imatinib treatments in C2C12 myotubes.

PGC 1α is known as one of the main regulators of mitochondrial biogenesis, and it translocates to the nucleus to induce the transcription of the nuclear encoded mitochondrial genes that play role in mitochondrial biogenesis and protein synthesis to cope with mitochondrial and cellular stress (Wu et al. 2016). It has been shown that increase in the PGC 1α level protects the cells from muscle atrophy and improves mitochondrial oxidative capacity, whereas decrease in PGC 1α leads to disruption of mitochondrial functions (VanderVeen et al. 2017). In this study, *PGC 1α* gene expression was significantly induced at high doses, the protein level of PGC 1α showed slight increase in the total cell lysate. However, PGC 1α protein level in nuclear fraction was observed to decrease significantly at the highest dose. This decrease in the nuclear PGC 1α may be interpreted as PGC 1α did not activate the protective mechanism after ripretinib exposure leading to cellular toxicity/-damage. Similarly, nuclear PGC 1α protein level has been shown to be inhibited in gentamicin-induced nephrotoxicity in renal cells (Negrette-Guzmán et al. 2015). It has also been found that the expression of PGC-1α mRNA and protein in skeletal muscle cells is impaired in heart diseases, type 2 diabetes, and aging (Jung and Kim, 2014; Panajatovic et al. 2020; Rowe et al. 2010). PGC 1α activates NRF 1 and NRF 2, and subsequently, the activated-NRF 2 induces PGC 1α and NRF 1. NRF 1 and NRF 2 transcription factors are also important in regulating nuclear encoded genes involved in mitochondrial functions and mitochondrial DNA transcription (Evans and Scarpulla, 1990; Gureev et al. 2019). Therefore, the PGC 1α/NRF 1/NRF 2 pathway is of great importance for cells to cope with mitochondrial stress. In this study, NRF 1 expression was decreased at both the protein and the gene levels dose-dependently. This suggests that PGC 1α could not activate mitochondrial biogenesis which may be associated with the disruption of the cytosol-nuclear signalization. VDAC1 is located in the outer mitochondrial membrane, and it plays roles in many cellular processes like transportation of ATP/ions/metabolites from cytosol to mitochondria or mitochondria to cytosol, apoptosis, calcium homeostasis etc. (Shoshan-Barmatz et al. 2017). ATP production and cell growth has been shown to be inhibited in VDAC1-deficient cells (Abu-Hamad et al. 2006). It has been found that the absence of VDAC1 in the skeletal muscle resulted in the decrease of complex IV activity (Anflous-Pharayra et al.

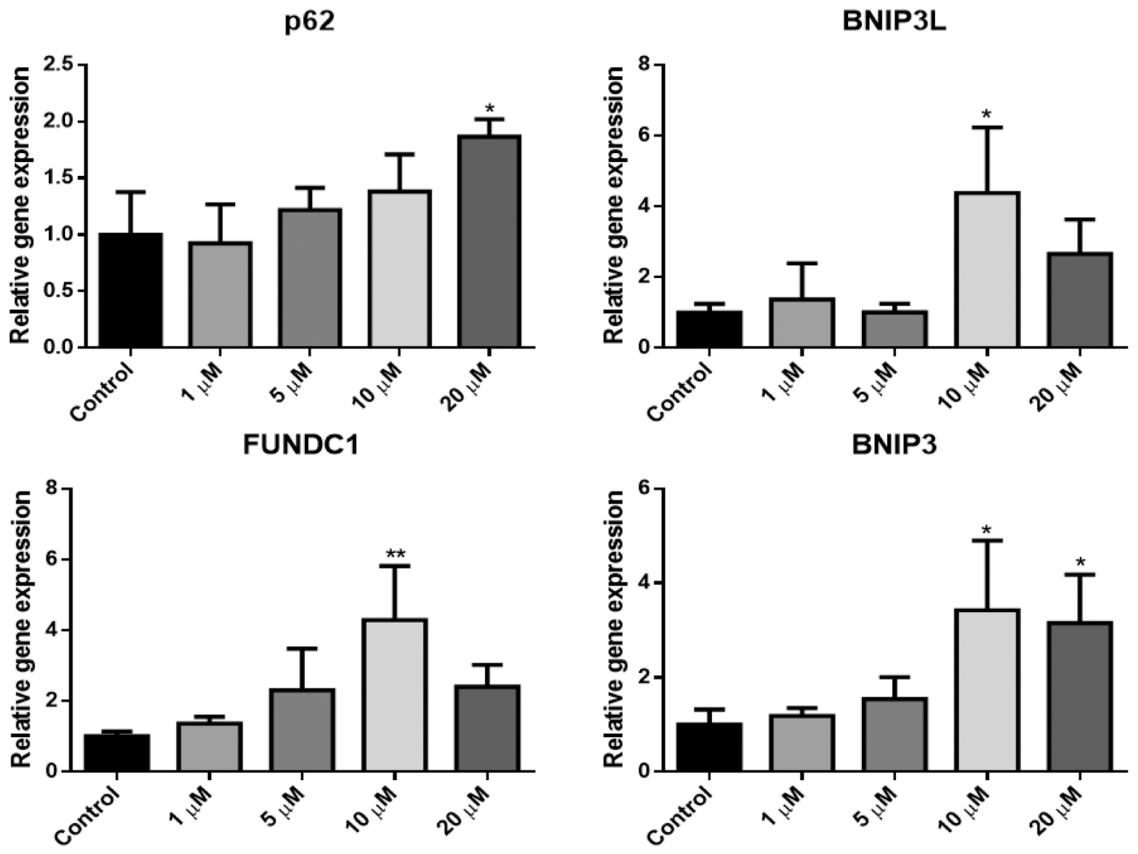

Fig. 6. Relative expressions of p62, BNIP3L, FUNDC1 and BNIP3 following 24 h ripretinib treatment. $*p < 0.05$, $**p < 0.01$ versus control group. BNIP3: BCL2/adenovirus E1B 19 kDa protein-interacting protein 3, BNIP3L: BCL2/adenovirus E1B 19 kDa protein-interacting protein 3-like, FUNDC1: FUN14 domain containing 1.

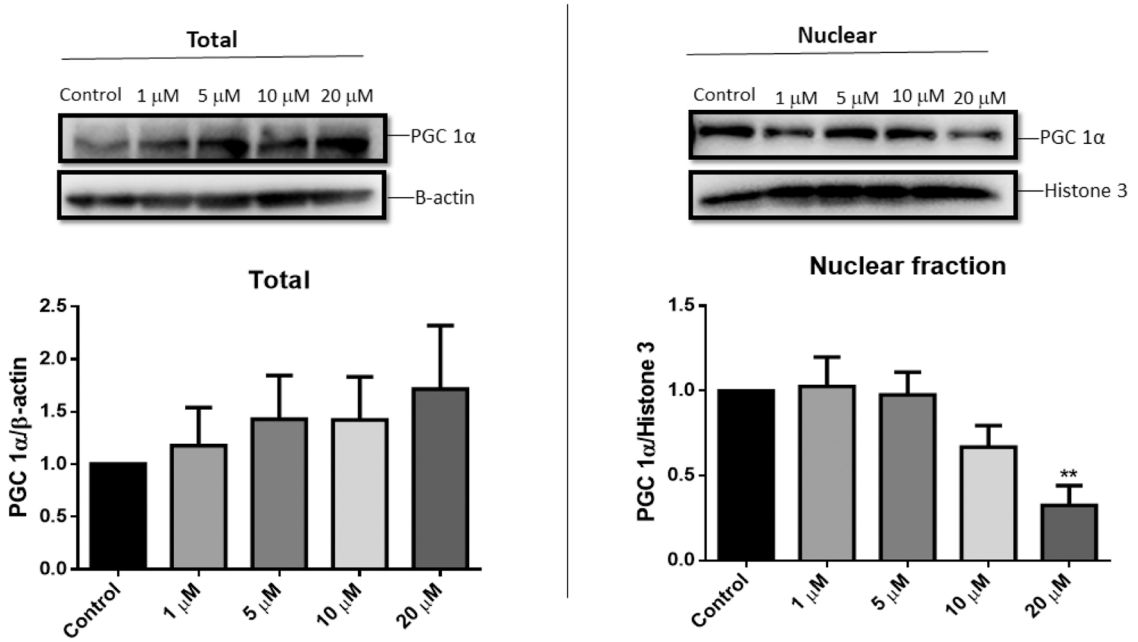

Fig. 7. PGC 1α expression in total cell lysate and nuclear fraction $**p < 0.01$ versus control group following 24 h ripretinib treatment. PGC 1α: Peroxisome proliferator-activated receptor gamma coactivator 1-alpha.

2011). According to our results, the reduced VDAC1 expression may have caused the disruption of complex IV activity which was observed following the highest ripretinib exposure. In addition, VDAC1 is also known as a mitochondrial mass marker (Schneider et al. 2022; Warren et al. 2020). In the present study, decrease in VDAC1 expression at the highest concentration could be considered as a sign of reduced

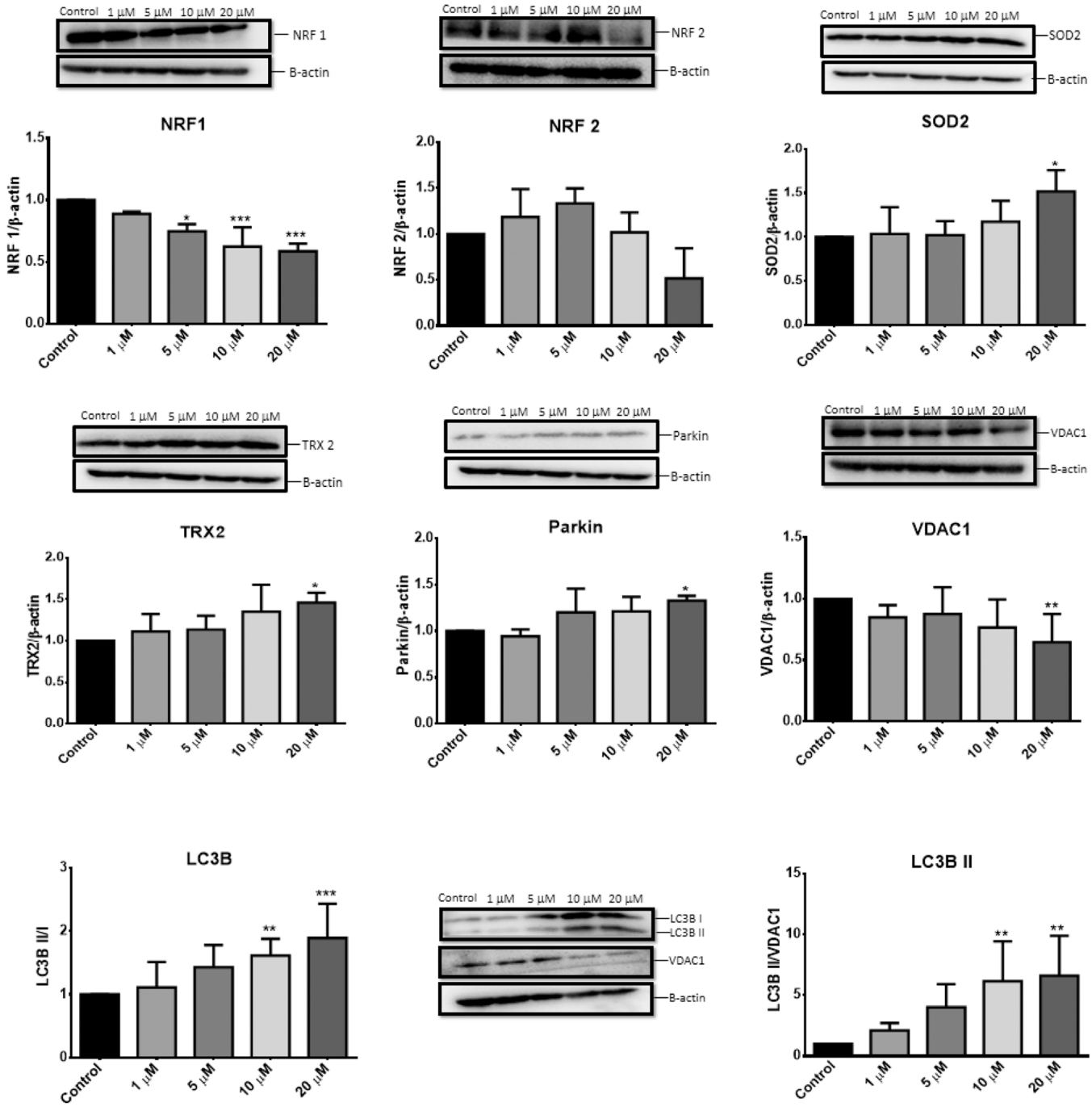

Fig. 8. Changes in the expression levels of NRF 1 NRF 2, SOD2, TRX2, Parkin, VDAC1 and LC3B proteins following 24 h ripretinib treatment. *$p < 0.05$, **$p < 0.01$, ***$p < 0.0001$ versus control group. NRF 1/2: Nuclear respiratory factor 1/2, SOD2: Superoxide dismutase, TRX2: Thioredoxin 2, LC3B: Microtubule associated protein light chain 3 beta, VDAC1: Voltage-dependent anion channel 1.

mitochondrial mass after ripretinib treatment.

The mtDNA copy number in a mitochondrion is important for the synthesis of proteins, which are important for proper functioning (Popov, 2020). For this reason, it is thought that mtDNA copy number can be used as a marker in the evaluation of mitochondrial function (Yue et al. 2018). The decrease in the amount of mtDNA causes an increase in dysfunctional mitochondria which can lead to various diseases (Tocchi et al. 2015). It has been determined that mtDNA and mitochondrial protein levels decrease in the skeletal muscle mitochondria with aging (Short et al. 2005). In the present study, the inhibitory effect of ripretinib on VDAC1 and mtDNA copy number indicated ripretinib-induced mitochondrial loss which is also in line with ATP depletion. Disruptions in mtDNA replication has been linked by mitochondrial diseases. POLG is a DNA polymerase enzyme that is responsible for mtDNA replication (Stumpf and Copeland, 2011). The conducted molecular docking study revealed that ripretinib has the potential to inhibit POLG. Besides, it was seen that the other tyrosine kinase inhibitor drugs approved for GIST including imatinib, sunitinib and regorafenib may also have notable interactions with POLG, giving high docking scores which were close to the positive control's docking score. Furthermore, since NRF 1/2 are important for mtDNA replication with regulating the mitochondrial transcription factors (Quan et al. 2020), the decrease in NRF 1 expression observed in this study might contribute to the reduction of the mtDNA replication and mtDNA copy number.

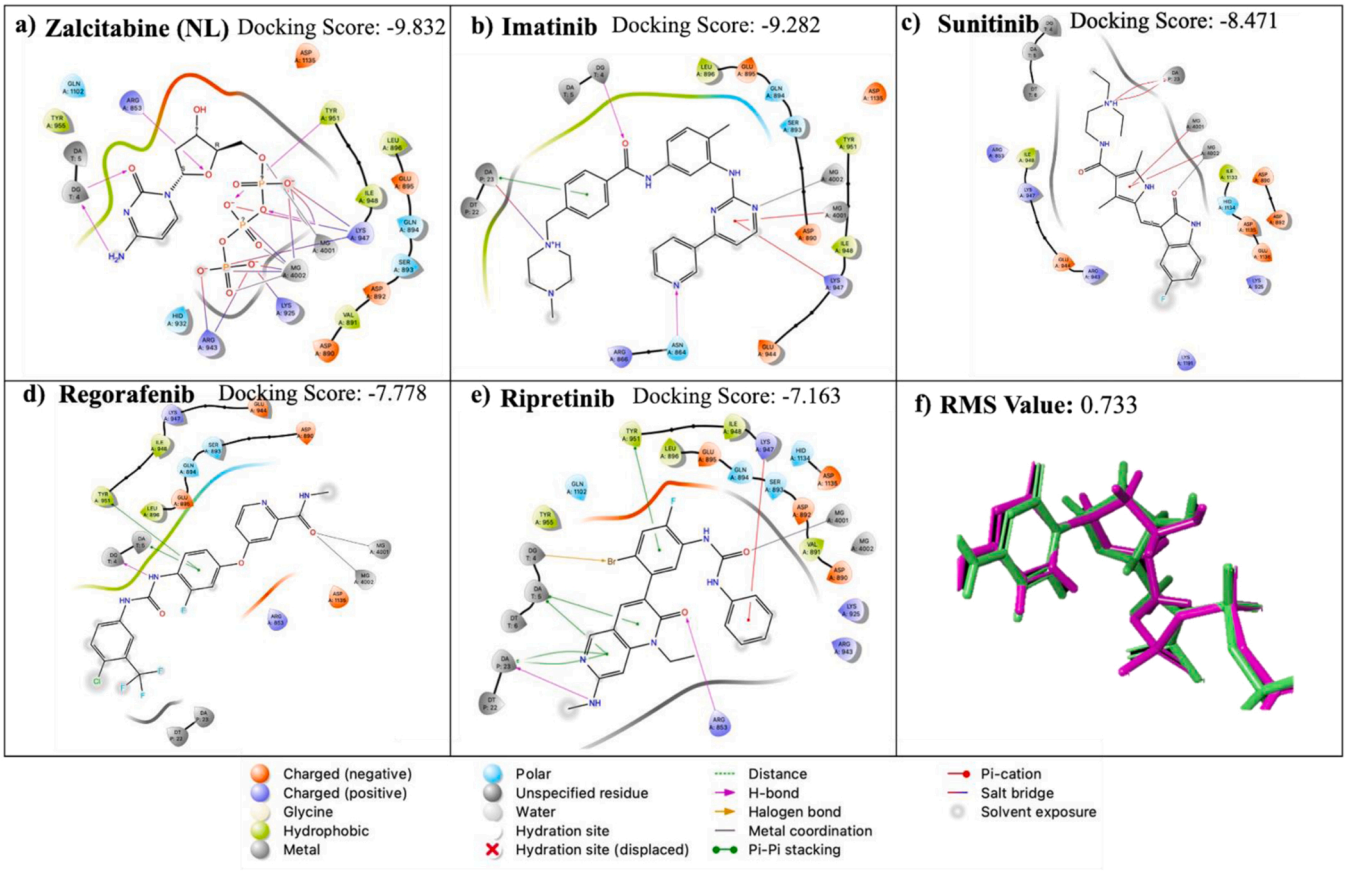

Fig. 9. Ligands and their 2D interactions with the active site of the crystal structure of POLG (PDB ID: 4ZTZ) (a-e). Validation of the docking model. Superposition of the docked pose (green) and experimental binding conformation (pink) of zalcitabine (2′-deoxycytidine-5′-triphosphate) in the binding pocket of 4ZTZ (f). NL: Native ligand, RMS: Root mean square.

Table 1
The docking scores of the molecules and their interactions with the active site of POLG enzyme crystal structure (PDB ID: 4ZTZ).

Ligand	Docking score, (kcal/mol)	H-bond	Pi-Pi stacking	Pi-cation	Salt bridge	Metal coordination
Zalcitabine (Native ligand)	-9.832	ARG853 TYR951 LYS947	-	-	ARG943 LYS925 LYS947 MG4001 MG4002	MG4001 MG4002
Imatinib	-9.282	ASN864	-	LYS947 MG4001	-	MG4002
Sunitinib	-8.471	-	-	MG4001 MG4002	-	MG4002
Regorafenib	-7.778	-	TYR951	-	-	MG4001 MG4002
Ripretinib	-7.163	ARG853	TYR951	LYS947	-	MG4001

Mitophagy, which is the removal of damaged mitochondria by autophagy, is also extremely important for maintaining cell homeostasis. It has been shown that age-related inhibition of mitophagy in skeletal muscle cells causes accumulation of damaged mitochondria and negatively affects muscle functions (Drake et al. 2017). Mitophagy is very important for the removal of damaged mitochondria, but on the other hand excessive mitophagy results in mitochondrial dysfunction and decrease in oxidative capacity of skeletal muscle cells in chronic diseases (Leermakers and Gosker, 2016). In autophagosomes, LC3 I is converted to LC3 II which is the phosphatidylethanolamine conjugated form of LC3 I (Guan et al. 2019). When the protein level ratios of LC3B II/I and LC3B II/VDAC1 are considered, both autophagy and mitophagy was observed to be increased after ripretinib treatment. LC3 is important for interaction of autophagosome and mitophagy proteins. Mitophagy can occur in cells either ubiquitin-mediated or receptor-mediated. p62, ubiquitin- and LC3-binding protein, plays role in ubiquitin-mediated mitophagy through PTEN-induced kinase 1 (Pink1)/Parkin. In damaged mitochondria Pink 1 stabilized outer surface of mitochondria and recruited Parkin to mitochondria. Parkin ubiquitinates mitochondrial proteins and the ubiquitinated proteins are recognized by p62. The ubiquitin chains with p62 interact with LC3-positive phagophores. Then, mitochondria are engulfed with autophagosome by membrane elongation (Guan et al. 2019, Saito and Sadoshima, 2015). In the present study, the expression of Parkin at the protein level and *p62* at the gene level were significantly elevated after ripretinib treatment. According to the results, Ripretinib might induce mitophagy through Pink/Parkin/p62 pathway in myotubes.

In receptor-mediated mitophagy, autophagy receptors play a role, i.e., BNIP3, BNIP3L, FUNDC1, which are located on the outer mitochondrial membrane. The interaction of these receptors with LC3 in the phagophore results in mitophagy (Guan et al. 2019; Harris et al. 2018). In the present study, the mitophagy-related genes (*BNIP3, BNIP3L,*

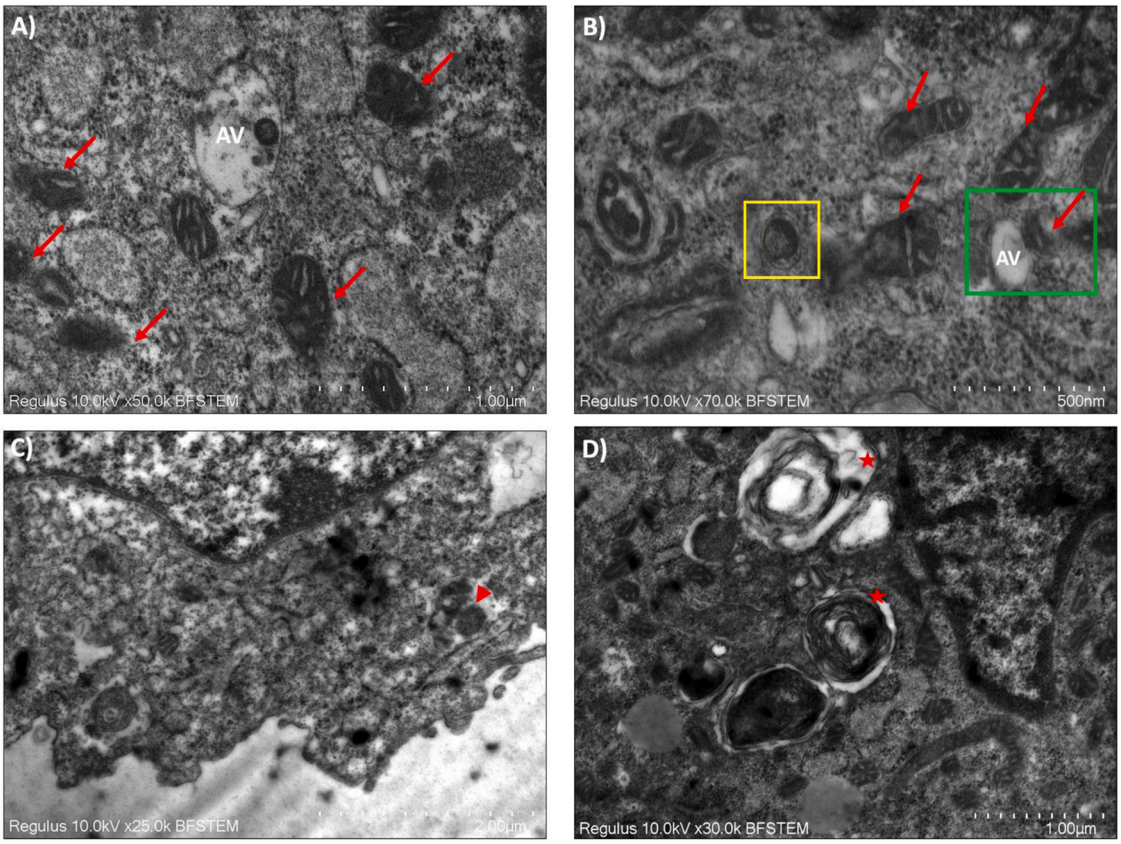

Fig. 10. TEM images following 20 μM ripretinib treatment for 24 h. Arrows are damaged mitochondria; arrowhead is autolysosomes containing damaged mitochondria; stars are concentrtic lamellar bodies; AV is autophagic vacuoles. It is shown the mitochondria engulfed with a membrane in yellow square and damaged mitochondrion fused with AV in green square.

FUNDC1) were upregulated after ripretinib treatment, which may be associated with the removal of damaged mitochondria to cope with cellular stress. Also, damaged mitochondria and mitophagic/autophagic structures were observed by electron microscope following ripretinib treatment. Similar to our results, regorafenib and sorafenib induced autophagy markers in the skeletal muscle (Huot et al. 2019). In cancer cachexia, mitochondrial oxidative metabolism and biogenesis have been known to be disrupted, and mitophagy to be induced in skeletal muscle cells, consequently leading to mitochondrial loss (Carson et al. 2016).

5. Conclusions

The present study revealed that mitochondrial damage could be one of underlying causes of skeletal muscle toxicity induced by ripretinib. In this regard, we observed that ripretinib induced ATP depletion, loss of MMP, increase in mtROS level and decrease in mtDNA copy number in the myotubes. While the PGC 1α/NRF 1/NRF 2 pathway, which is involved in mitochondrial biogenesis, was not activated; mitophagy was induced following ripretinib treatment, which may be associated with the mitochondrial loss. Long-term and clinical studies are still needed to understand skeletal muscle toxicity induced by ripretinib treatment.

The severity and frequency of toxic effects might be proportional to the increase in the population using the drug ripretinib. For this reason, it is of great importance to determine the mechanisms of the drug-induced toxic effect mechanisms. The elucidation of the mechanisms of toxic effects on the skeletal muscle could provide a foresight for the development of new treatment strategies and help reduce the toxic effects of the drug on the skeletal muscle by trying new approaches; thus, preventing the interruption of successful drug therapy.

Declaration of Competing Interest

The authors declare that they have no known competing financial interests or personal relationships that could have appeared to influence the work reported in this paper.

Data availability

Data will be made available on request.

Acknowledgments

This study was supported by Scientific Research Project Coordination Unit of Istanbul University. Project number: TSA-2021–37953 and FBG-2021–37896.

Appendix A. Supporting information

Supplementary data associated with this article can be found in the online version at doi:10.1016/j.tox.2023.153489.

References

Abu-Hamad, S., Sivan, S., Shoshan-Barmatz, V., 2006. The expression level of the voltage-dependent anion channel controls life and death of the cell. Proc. Natl. Acad. Sci. USA 103, 5787–5792. https://doi.org/10.1073/PNAS.0600103103.

Anflous-Pharayra, K., Lee, N., Armstrong, D.L., Craigen, W.J., 2011. VDAC3 has differing mitochondrial functions in two types of striated muscles. Biochim. Biophys. Acta Bioenergy 1807 (1), 150–156. https://doi.org/10.1016/j.bbabio.2010.09.007.

Atashbar, S., Jamali, Z., Khezri, S., Salimi, A., 2022. Celecoxib decreases mitochondrial complex IV activity and induces oxidative stress in isolated rat heart mitochondria: An analysis for its cardiotoxic adverse effect. J. Biochem. Mol. Toxicol. 36 (1), e22934 https://doi.org/10.1002/jbt.22934.

Bouitbir, J., Panajatovic, M.V., Frechard, T., Roos, N.J., Krähenbühl, S., 2020. Imatinib and dasatinib provoke mitochondrial dysfunction leading to oxidative stress in C2C12 myotubes and human RD cells. Front. Pharmacol. 11, 1106. https://doi.org/10.3389/FPHAR.2020.01106/FULL.

Carson, J., Hardee, J., VanderVeen, B., 2016. The emerging role of skeletal muscle oxidative metabolism as a biological target and cellular regulator of cancer-induced muscle wasting. Semin. Cell Dev. Biol. 54, 53–67. https://doi.org/10.1016/j.semcdb.2015.11.005.

Damaraju, V., Kuzma, M., Cass, C., Putman, C.T., Sawyer, M.B., 2018. Multitargeted kinase inhibitors imatinib, sorafenib and sunitinib perturb energy metabolism and cause cytotoxicity to cultured C2C12 skeletal muscle derived. Biochem. Pharmacol. 155, 162–171. https://doi.org/10.1016/j.bcp.2018.07.001.

Drake, J.C., Yan, Z., Drake, J.C., Yan, Z., 2017. Mitophagy in maintaining skeletal muscle mitochondrial proteostasis and metabolic health with ageing. Wiley Online Libr. 595, 22–26. https://doi.org/10.1113/JP274337.

Evans, M., Scarpulla, R.C., 1990. NRF-1: a trans-activator of nuclear-encoded respiratory genes in animal cells. Genes Dev. 4 (6), 1023–1034. https://doi.org/10.1101/gad.4.6.1023.

FDA and CDER , 2020. Highlights of prescribing information. ⟨https://www.accessdata.fda.gov/drugsatfda_docs/label/2020/213973s000lbl.pdf⟩ (accessed May 30, 2022).

Friesner, R.A., Banks, J.L., Murphy, R.B., Halgren, T.A., Klicic, J.J., Mainz, D.T., Repasky, M.P., Knoll, E.H., Shelley, M., Perry, J.K., Shaw, D.E., Francis, P., Shenkin, P.S., 2004. Glide: a new approach for rapid, accurate docking and scoring. 1. Method and assessment of docking accuracy. J. Med. Chem. 47, 1739–1749. https://doi.org/10.1021/jm0306430.

Friesner, R.A., Murphy, R.B., Repasky, M.P., Frye, L.L., Greenwood, J.R., Halgren, T.A., Sanschagrin, P.C., Mainz, D.T., 2006. Extra precision glide: docking and scoring incorporating a model of hydrophobic enclosure for protein− ligand complexes. J. Med. Chem. 49, 6177–6196. https://doi.org/10.1021/jm051256o.

Gouspillou, G., Hepple, R.T., 2016. Editorial: mitochondria in skeletal muscle health, aging and diseases. Front. Physiol. 7, 446. https://doi.org/10.3389/FPHYS.2016.00446/FULL.

Guan, Y., Drake, J., Yan, Z., 2019. Exercise-induced mitophagy in skeletal muscle and heart. Exerc Sport Sci. Rev. 47 (3), 151. https://doi.org/10.1249/JES.0000000000000192.

Gureev, A.P., Shaforostova, E.A., Popov, V.N., 2019. Regulation of mitochondrial biogenesis as a way for active longevity: Interaction between the Nrf2 and PGC-1α signaling pathways. Front. Genet. 10, 435. https://doi.org/10.3389/FGENE.2019.00435/FULL.

Halgren, T.A., Murphy, R.B., Friesner, R.A., Beard, H.S., Frye, L.L., Thomas Pollard, W., Banks, J.L., 2004. Glide: a new approach for rapid, accurate docking and scoring. 2. Enrichment factors in database screening. J. Med. Chem. 47, 1750–1759. https://doi.org/10.1021/jm030644s.

Harris, J., Deen, N., Zamani, S., Hasnat, M.A., 2018. Mitophagy and the release of inflammatory cytokines. Mitochondrion 41, 2–8. https://doi.org/10.1016/j.mito.2017.10.009.

Hartmann, J., Haap, M., Kopp, H.S., Lipp, H.S., 2009. Tyrosine kinase inhibitors-a review on pharmacology, metabolism and side effects. Curr. Drug Metab. 10 (5), 470–481. https://doi.org/10.2174/138920009788897975.

Huot, J., Essex, A., Gutierrez, M., Barreto, R., Wang, M., Waning, D.L., Plotkin, L.I., Bonetto, A., 2019. Chronic treatment with multi-kinase inhibitors causes differential toxicities on skeletal and cardiac muscles. Cancers 11 (4), 571. https://doi.org/10.3390/cancers11040571.

Jung, S., Kim, K., 2014. Exercise-induced PGC-1α transcriptional factors in skeletal muscle. Integr. Med. Res. 3 (4), 155–160. https://doi.org/10.1016/j.imr.2014.09.004.

Kaminski, J., Lançon, A., Aires, V., Limagne, E., Tili, E., Michaille, J.J., Latruffe, N., 2012. Resveratrol initiates differentiation of mouse skeletal muscle-derived C2C12 myoblasts. Biochem. Pharmacol. 84 (10), 1251–1259. https://doi.org/10.1016/j.bcp.2012.08.023.

Kokoszka, J.E., Coskun, P., Esposito, L.A., Wallace, D.C., 2001. Increased mitochondrial oxidative stress in the Sod2 (+/−) mouse results in the age-related decline of mitochondrial function culminating in increased apoptosis. Proc. Natl. Acad. Sci. USA 98 (5), 2278–2283. https://doi.org/10.1073/pnas.051627098.

Kumar, S., Philip, A., Pavithran, K., 2021. Ripretinib: a narrative drug review. Drug Rev. 4 (1), 93–98. https://doi.org/10.4103/crst.crst_308_20.

Kunz, W.S., 2001. Control of oxidative phosphorylation in skeletal muscle. Biochim Biophys. Acta Bioenergy 1504, 12–19. https://doi.org/10.1016/S0005-2728(00)00235-8.

Leermakers, P., Gosker, H.R., 2016. Skeletal muscle mitophagy in chronic disease: implications for muscle oxidative capacity? Curr. Opin. Clin. Nutr. Metab. Care 19 (6), 427–433. https://doi.org/10.1097/MCO.0000000000000319.

Livak, K., Schmittgen, T.D., 2001. Analysis of relative gene expression data using real-time quantitative PCR and the 2− ΔΔCT method. Methods 25 (4), 402–408. https://doi.org/10.1006/meth.2001.1262.

Madhavi Sastry, G., Adzhigirey, M., Day, T., Annabhimoju, R., Sherman, W., 2013. Protein and ligand preparation: parameters, protocols, and influence on virtual screening enrichments. J. Comput. Aided Mol. Des. 27, 221–234. https://doi.org/10.1007/S10822-013-9644-8.

Martínez, M., García, A., Luzardo, E., Chávez-Castillo, M., Olivar, J.C., Salazar, J., Valesco, M., Quintero, J.J.R., Bermúdez, V., 2017. Energetic metabolism in cardiomyocytes: molecular basis of heart ischemia and arrhythmogenesis. Vessel 2, 32. https://doi.org/10.20517/2574-1209.2018.68.

Min, K., Smuder, A.J., Kwon, O.S., Kavazis, A.N., Szeto, H.H., Powers, S.K., 2011. Mitochondrial-targeted antioxidants protect skeletal muscle against immobilization-induced muscle atrophy. J. Appl. Physiol. 111, 1459–1466. https://doi.org/10.1152/JAPPLPHYSIOL.00591.2011.

Murphy, E., Ardehali, H., Balaban, R.S., DiLisa, F., Dorn, G.W., Kitsis, R.N., Otsu, K., Ping, P., Rizzuto, R., Sack, M.N., Wallace, D., Youle, R.J., 2016. Mitochondrial function, biology, and role in disease: a scientific statement from the American heart association. Circ. Res. 118, 1960–1991. https://doi.org/10.1161/RES.0000000000000104.

Murphy, M.P., 2009. How mitochondria produce reactive oxygen species. Biochem. J. 417 (1), 1–13. https://doi.org/10.1042/BJ20081386.

Napolitano, G., Fasciolo, G., Venditti, P., 2021. Mitochondrial management of reactive oxygen species. Antioxidants 10 (11), 1824. https://doi.org/10.3390/antiox10111824.

Negrette-Guzmán, M., García-Niño, W.R., Tapia, E., Zazueta, C., Huerta-Yepez, S., León-Contreras, J.C., Hernández-Pando, R., Aparicio-Trejo, O.E., Madero, M., Pedraza-Chaverri, J., 2015. Curcumin attenuates gentamicin-induced kidney mitochondrial alterations: possible role of a mitochondrial biogenesis mechanism. Evid. Based Complement. Altern. Med. https://doi.org/10.1155/2015/917435.

Okada, N., Yako, T., Nakamura, S., Shimazawa, M., Hara, H., 2021. Reduced mitochondrial complex II activity enhances cell death via intracellular reactive oxygen species in STHdhQ111 striatal neurons with mutant huntingtin. J. Pharmacol. Sci. 147 (4), 367–375. https://doi.org/10.1016/j.jphs.2021.09.001.

Okamoto, S., Asgar, N., Yokota, S., Saito, K., Minokoshi, Y., 2019. Role of the α2 subunit of AMP-activated protein kinase and its nuclear localization in mitochondria and energy metabolism-related gene expressions in. Metabolism 90, 52–68. https://doi.org/10.1016/j.metabol.2018.10.003.

Panajatovic, M., Singh, F., Krähenbühl, S., Boutbir, J., 2020. Simvastatin impairs glucose homeostasis in mice depending on PGC-1α skeletal muscle expression. Biomedicines 8 (9), 351. https://doi.org/10.3390/biomedicines8090351.

Popov, L.D., 2020. Mitochondrial biogenesis: an update. J. Cell Mol. Med. 24, 4892–4899. https://doi.org/10.1111/JCMM.15194.

Quan, Y., Xin, Y., Tian, G., Zhou, J., Liu, X., 2020. Mitochondrial ROS-modulated mtDNA: a potential target for cardiac aging. Oxid. Med. Cell. Longev. https://doi.org/10.1155/2020/9423593.

Quiros, P.M., Goyal, A., Jha, P., Auwerx, J., 2017. Analysis of mtDNA/nDNA Ratio in Mice. Curr. Protoc. Mouse Biol. 7, 47–54. https://doi.org/10.1002/CPMO.21.

Rao, J., Wu, Y., Fan, X., Yang, S., Jiang, L., Dong, Z., Chen, S., 2022. Facilitating Mitophagy via Pink1/Parkin2 Signaling Is Essential for the Neuroprotective Effect of β-Caryophyllene against CIR-Induced Neuronal Injury. Brain Sci. 12 (7), 868. https://doi.org/10.3390/brainsci12070868.

Rinninella, E., Cintoni, M., Raoul, P., Ponziani, F.R., Pompili, M., Pozzo, C., Strippoli, A., Bria, E., Tortora, G., Gasbarrini, A., Mele, M.C., 2021. Prognostic value of skeletal muscle mass during tyrosine kinase inhibitor (TKI) therapy in cancer patients: a systematic review and meta-analysis. Intern. Emerg. Med. 16, 1341–1356. https://doi.org/10.1007/S11739-020-02589-5.

Romanello, V., Sandri, M., 2016. Mitochondrial quality control and muscle mass maintenance. Front. Physiol. 6, 422. https://doi.org/10.3389/FPHYS.2015.00422/FULL.

Rowe, G.C., Jiang, A., Arany, Z., 2010. PGC-1 coactivators in cardiac development and disease. Circ. Res. 107, 825–838. https://doi.org/10.1161/CIRCRESAHA.110.223818.

Saito, T., Sadoshima, J., 2015. Molecular mechanisms of mitochondrial autophagy/mitophagy in the heart. Circ. Res. 116 (8), 1477–1490. https://doi.org/10.1161/CIRCRESAHA.116.303790.

Schneider, A., Özsoy, M., Zimmermann, F.A., Brunner, S., Feichtinger, R., Mayr, J., Kofler, B., Neureiter, D., Klieser, E., Aigner, E., et al., 2022. Expression of oxidative phosphorylation complexes and mitochondrial mass in pediatric and adult inflammatory bowel disease. Oxid. Med. Cell. Longev. https://doi.org/10.1155/2022/9151169.

Short, K.R., Bigelow, M.L., Kahl, J., Singh, R., Coenen-Schimke, J., Raghavakaimal, S., Nair, K.S., 2005. Decline in skeletal muscle mitochondrial function with aging in humans. Proc. Natl. Acad. Sci. USA 102, 5618–5623. https://doi.org/10.1073/PNAS.0501559102.

Shoshan-Barmatz, V., De, S., Meir, A., 2017. The mitochondrial voltage-dependent anion channel 1, Ca2+ transport, apoptosis, and their regulation. Front. Oncol. 7, 60. https://doi.org/10.3389/FONC.2017.00060/FULL.

Sivandzade, F., Bhalerao, A., Cucullo, L., 2019. Analysis of the mitochondrial membrane potential using the cationic JC-1 dye as a sensitive fluorescent probe. Bio Protoc. 9 (1) https://doi.org/10.21769/BioProtoc.3128.

Stumpf, J.D., Copeland, W.C., 2011. Mitochondrial DNA replication and disease: Insights from DNA polymerase γ mutations. Cell. Mol. Life Sci. 68, 219–233. https://doi.org/10.1007/S00018-010-0530-4.

Szymanski, M.R., Kuznetsov, V.B., Shumate, C., Meng, Q., Lee, Y., Patel, G., Patel, S., Yin, Y.W., 2015. Structural basis for processivity and antiviral drug toxicity in human mitochondrial DNA replicase. EMBO J. 34, 1959–1970. https://doi.org/10.15252/EMBJ.201591520.

Tocchi, A., Quarles, E., Basisty, N., Gitari, L., Rabinovitch, P.S., 2015. Mitochondrial dysfunction in cardiac aging. Biochim. Biophys. Acta 1847 (11), 1424–1433. https://doi.org/10.1016/j.bbabio.2015.07.009.

VanderVeen, B., Fix, D., Carson, J., 2017. Disrupted skeletal muscle mitochondrial dynamics, mitophagy, and biogenesis during cancer cachexia: a role for inflammation. Oxid. Med. Cell. Longev. https://doi.org/10.1155/2017/3292087.

Warren, C., McDonald, D., Capaldi, R., Deehan, D., Taylor, R.W., Filby, A., Turnbull, D. M., Lawless, C., Vincent, A.E., 2020. Decoding mitochondrial heterogeneity in single muscle fibres by imaging mass cytometry. Sci. Rep. 10 (1), 15336 https://doi.org/10.1038/s41598-020-70885-3.

Wong, C.Y., Al-Salami, H., Dass, C.R., 2020. C2C12 cell model: its role in understanding of insulin resistance at the molecular level and pharmaceutical development at the preclinical stage. J. Pharm. Pharmacol. 72 (12), 1667–1693. https://doi.org/10.1111/jphp.13359.

Wu, K., Wu, C., Chao, Y., Hung, C.Y., Chan, J., 2016. Impaired Nrf2 regulation of mitochondrial biogenesis in rostral ventrolateral medulla on hypertension induced by systemic inflammation. Free Radic. Biol. 97, 58–74. https://doi.org/10.1016/j.freeradbiomed.2016.05.012.

Yue, P., Jing, S., Liu, L., Ma, F., Zhang, Y., Wang, C., Duan, H., Zhou, K., Hua, Y., Wu, G., Li, Y., 2018. Association between mitochondrial DNA copy number and cardiovascular disease: Current evidence based on a systematic review and meta-analysis. PLOS One 13 (11), e0206003. https://doi.org/10.1371/JOURNAL.PONE.0206003.

Zorova, L.D., Popkov, V.A., Plotnikov, E.Y., Silachev, D.N., Pevzner, I.B., Jankauskas, S. S., Babenko, V.A., Zorov, S.D., Balakireva, A. v, Juhaszova, M., Sollott, S.J., Zorov, D. B., 2018. Mitochondrial membrane potential. Anal. Biochem. 552, 50–59. https://doi.org/10.1016/J.AB.2017.07.009.

GIST Support International. 2020. Switch Pocket Kinase Inhibitors. ⟨https://www.gistsupport.org/ask-the-professional/switch-pocket-kinase-inhibitors/⟩ (accessed 7.21.22).